Biomedical Signal Processing and Control 104 (2025) 107506

Contents lists available at ScienceDirect

Biomedical Signal Processing and Control

journal homepage: www.elsevier.com/locate/bspc

Kalman filter soft sensor to handle signal quality loss in closed-loop controlled anesthesia

Ylva Wahlquist [a,*], Nicola Paolino [b], Michele Schiavo [b], Antonio Visioli [b], Kristian Soltesz [a]

[a] Lund University, Department of Automatic Control, Sweden
[b] University of Brescia, Department of Mechanical and Industrial Engineering, Italy

ARTICLE INFO

Keywords:
Closed-loop anesthesia
Kalman filter
PID control

ABSTRACT

Background and objective: This study aims to enhance the performance of a closed-loop anesthetic depth control system by fusing noise-corrupted clinical measurements with a non-perfect pharmacological model.
Methods: We implement a Kalman filter to constitute a trade-off between model prediction and measurement signal dependence for depth of hypnosis (DoH) control using a previously evaluated PID controller. This trade-off is adjusted online, based on signal quality index (SQI) feedback, provided by the clinical DoH monitor, in this case assumed to be the bispectral index (BIS) monitor.
Results: Our simulations show that the proposed solution leads to fundamental performance improvements over the traditional monitor feedback case, which fails to provide the required clinical performance when the SQI drops due to signal inference. In particular, the soft sensor approach increases the time of DoH within the recommended clinical range of 40–60 BIS from 71% to 99%, compared to simple feedback of the noisy monitor output.
Conclusion: Our Kalman filter soft-sensor approach succeeds in importantly increasing system robustness to measurement signal disturbances by combining sensor measurements and model predictions.

1. Introduction

A key challenge in general anesthesia is to adequately control the depth of hypnosis (DoH) in the patient [1]. In this paper, we consider DoH control using the intravenously infused drug propofol. The control is challenging, since DoH cannot be measured directly, but is only observed indirectly through correlated signals and patient signs. In addition to manual titration, two computer-controlled dosing regimens have gained ground.

Of these, target-controlled infusion (TCI) [2] has received the broadest clinical acceptance to date. TCI is a model-based feed-forward strategy, that optimizes an infusion trajectory offline, based on a user-provided reference. As such, it is vulnerable both to model errors and external disturbances, since the infusion is not based on actual measurements of the patient state. However, if the anesthesiologist suspects model errors or disturbances based on patient observations, they can update the setpoint concentration.

The other computer-controlled dosing strategy that has to date been employed in several research studies is closed-loop control. It relies on feedback from a DoH estimate, provided by a non-invasive processed electroencephalogram (pEEG) monitor [3]. Such monitors report DoH on the bispectral index (BIS) scale, where 100 is the maximum achievable cortical activity (being awake corresponds to a value near 100), and 0 represents an iso-electric EEG (corresponding to the maximally achievable DoH) [4].

Closed-loop systems are well known to outperform open-loop ones when suitably designed and tuned. That is why several research efforts have been made to design closed-loop architectures, as demonstrated by [5–7]. The closed-loop control algorithm could be a simple proportional–integrative–derivative (PID) [8] controller as in [9–13], or some more advanced one as in e.g., [14–20]. We have previously shown that the control performance of these systems is mainly limited by the modeling uncertainties such as those coming from inter- and intra-patient variability, rather than by the choice of control algorithm [10,21]. Hence, we base our example on a PID-controlled system, although the methodology we introduce is equally applicable to other types of controllers. While closed-loop systems provide some means

* Correspondence to: Department of Automatic Control, Lund University, SE-221 00, Lund, Sweden.
E-mail addresses: ylva.wahlquist@control.lth.se (Y. Wahlquist), nicola.paolino@unibs.it (N. Paolino), michele.schiavo@unibs.it (M. Schiavo), antonio.visioli@unibs.it (A. Visioli), kristian.soltesz@control.lth.se (K. Soltesz).

https://doi.org/10.1016/j.bspc.2025.107506
Received 18 June 2024; Received in revised form 10 December 2024; Accepted 2 January 2025
Available online 15 January 2025

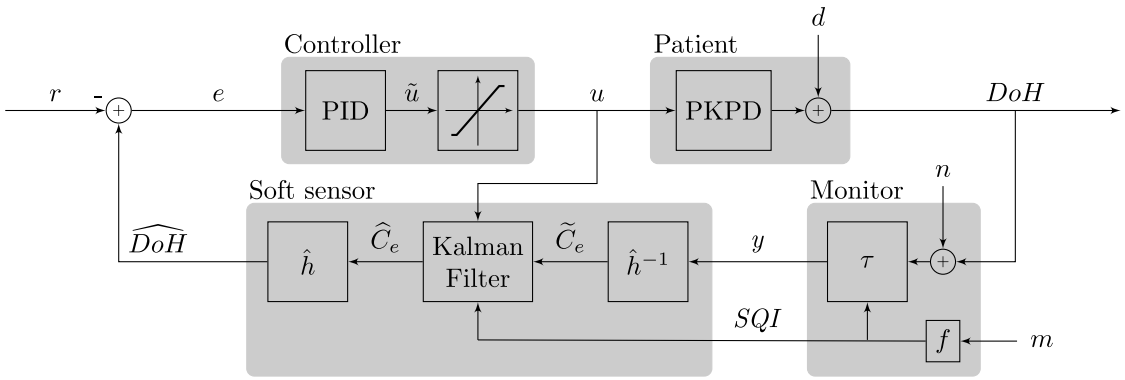

Fig. 1. Control scheme featuring the proposed Kalman-filter-based soft sensor (bottom left shaded box). The components are described one by one in Sections 2.1 to 2.4. The objective is to follow the *DoH* reference r, by adequately titrating the infusion rate u, in presence of surgical disturbance d, measurement noise n, electric monitor inference m, and imperfection of the patient model.

to attenuate external disturbances and cope with model errors, they are vulnerable to corruption of the measurement that constitutes the feedback signal.

Alongside a *DoH* estimate, clinical *DoH* monitors provide a signal quality index (*SQI*) ranging from 0–100 (low–high signal quality). This index, which is updated and displayed on the monitor, provides the anesthesiologist with an estimate of the current BIS measurement reliability. In clinical practice, a *DoH* measure associated with an $SQI \leq 50$ is considered unreliable [22]. Signal quality loss directly affects the anesthesiologist's working procedure since they cannot rely on the *DoH* monitor while adjusting the drug infusion rate. Low *SQI* values are common during general surgery [23,24]. This can, for example, be due to forehead motion, improper sensor placement, or electrical inference from the use of an electro-scalpel [25].

We consider a scenario where the monitor *DoH* estimate is corrupted by inference. By introducing a novel soft-sensor approach to closed-loop controlled anesthesia, we can maintain patient safety despite loss of signal quality. This is achieved by a Kalman filter, a classic methodology that has been only recently exploited in biomedical and biomechanical engineering [26,27]. In particular, the usage of a Kalman filter in the anesthesia field has been proposed in, for example, [28] to estimate both the state and parameters of the system to predict the future trajectory. Here, a linear Kalman filter is used to shift the balance from measurement to model reliance (i.e., from ordinary closed-loop towards TCI), when *SQI* is decreased. When signal quality is good (*SQI* closer to 100), feedback will essentially be based on the monitor output, as in conventional closed-loop controlled anesthesia. In contrast, when signal quality is poor (*SQI* closer to 0), the feedback will be based mainly on the model prediction, and effectively behave like TCI.

In this work, we introduce a novel Kalman-filter-based soft-sensor concept for anesthesia control. To demonstrate this methodology, we use a patient simulator that explicitly models both patient variability (model uncertainty), measurement disturbances that our model-based soft-sensor is purposed to attenuate, and measurement noise.

The novelty of our approach thus lies in using the Kalman filter as a tuning knob to shift between model and measurement reliance, rather than as the minimum-variance estimator where its tuning parameters are optimized to minimize estimation error, assuming some Gaussian state and measurement noise processes.

2. System architecture

Our proposed closed-loop control architecture is shown in Fig. 1. It consists of four main components: the patient dynamics (Section 2.1), the Kalman-filter-based soft sensor (Section 2.2), the clinical *DoH* monitor (Section 2.3), and the drug-dosing closed-loop controller (Section 2.4).

2.1. Patient

Kalman filtering is a model-based approach, and in our case, patient dynamics are modeled by a conventional four-compartment linear pharmacological model [21,29,30]. These linear models are the gold standard to represent propofol pharmacokinetics and they have been employed in commercial devices, such as in TCI [31]. Precisely, the model is defined as

$$\dot{\boldsymbol{x}}(t) = A\boldsymbol{x}(t) + Bu(t), \tag{1a}$$

$$C_e(t) = C\boldsymbol{x}(t), \tag{1b}$$

where

$$A = \begin{bmatrix} -(k_{10}+k_{12}+k_{13}) & k_{21} & k_{31} & 0 \\ k_{12} & -k_{21} & 0 & 0 \\ k_{13} & 0 & -k_{31} & 0 \\ \frac{k_{e0}}{V_1} & 0 & 0 & -k_{e0} \end{bmatrix}, \tag{2a}$$

$$B = \begin{bmatrix} 1 & 0 & 0 & 0 \end{bmatrix}^\top, \tag{2b}$$

$$C = \begin{bmatrix} 0 & 0 & 0 & 1 \end{bmatrix}. \tag{2c}$$

The system in (1) represents a linear system since the right-hand sides of (1a) and (1b) are both linear functions of the state $\boldsymbol{x}$ and input u.

Propofol infusion is modeled by the input signal u [mg s^{-1}]. The first state component, x_1 [mg], represents the mass of propofol in the blood plasma, while the last, $x_4 = C_e$ [mg L^{-1}], models the effect-site concentration, being the drug concentration in the cortex of the brain. The other state components, x_2 [mg] and x_3 [mg], model the mass distribution in fast and slow tissue, respectively. The parameters k_{10}, k_{12}, k_{13}, k_{21}, k_{31}, and k_{e0}, in units of s^{-1}, are rate constants, and V_1 [L] models the blood plasma volume. Note that the effect-site concentration, or any of the other states, is not directly measurable.

Saturation effects at low and high effect-site drug concentrations are modeled using a Hill sigmoid output nonlinearity [32]

$$DoH(t) = h(C_e(t); \gamma, C_{e50}, E_0, E_{\max}) = E_0 - E_{\max}\frac{C_e(t)^\gamma}{C_e(t)^\gamma + C_{e50}^\gamma}. \tag{3}$$

The *DoH* level in the absence of a drug is $E_0 \lessapprox 100$ BIS, and the maximum deviation from this level is $E_{\max} \lessapprox 100$ BIS. The effect-site concentration C_{e50} [mg L^{-1}] is the concentration at which the hypnotic depth is halfway between the limits defined through E_0 and $E_{\max}$, $DoH = E_0 - E_{\max}/2$. The third parameter of (3), γ, is a unitless shape parameter that defines the steepness of the sigmoid, such that the limit $\gamma \to \infty$ defines a *DoH* step between E_0 and $E_0 - E_{\max}$ at $C_e = C_{e50}$. Together, (2) and (3) constitutes a so-called pharmacokinetic–pharmacodynamic (PKPD) model, as thoroughly introduced and explained in [21].

Since we will use our model in a closed-loop interconnection with a periodically sampled controller, we will use the approximation-error-free zero-order-hold discretization of (2). Denoting the sampling period

$T_s = 1$ s, we index the samples so that if $\boldsymbol{x}(t) = \boldsymbol{x}_k$, then $\boldsymbol{x}(t+T_s) = \boldsymbol{x}_{k+1}$. This results in the discrete state space representation

$$\boldsymbol{x}_{k+1} = F\boldsymbol{x}_k + Gu_k, \tag{4a}$$

$$(C_e)_k = H\boldsymbol{x}_k, \tag{4b}$$

with constant matrices $F = \exp(AT_s)$, $G = \int_0^{T_s} \exp(As)\, ds\, B$, and $H = C$, as derived and explained in [33]. The input at sample k is denoted u_k.

The drug response dynamics vary between patients and are commonly modeled with fixed and random effects. The fixed effects model the variability that can be explained by covariates such as age, height, and weight. The random effects model the remaining variability that is not explained by covariates [21]. This is a well-established methodology for modeling dynamic uncertainty in the drug response.

For a particular model parameter θ with fixed effect (nominal) value θ_0, the parameter is assumed to be drawn from the log-normal distribution

$$\theta = \theta_0 \exp(\eta_p), \tag{5}$$

where the random effect η_p is a normal stochastic variable with zero mean and variance σ_p^2 [34].

To reflect this, we use the Schnider population model [29], which expresses the model parameters mentioned in the individual patient covariates age, height, weight, and gender. The Schnider model incorporates intra-patient variability (i.e., random effects) through coefficients of variation (CV). The variances σ_θ^2 of the PK parameter θ relates to the corresponding CV_θ through [35]

$$\sigma_\theta^2 = \log\left(\left(\frac{CV_\theta}{100}\right)^2 + 1\right). \tag{6}$$

Surgical stimulation typically increases the level of awareness in the patient, thus affecting DoH. It is customary [21,36] to model the effect of such stimulation as an additive disturbance d, acting on DoH, as shown in Fig. 1.

2.2. Soft sensor

The Kalman filter is an optimal state estimator, in the sense that it provides the state estimate that minimizes error variance, given that the system dynamics are linear and the noise is Gaussian [37].

While the Hill function (3) is non-linear, it is invertible. Particularly, if we equate the right-hand-side of (3) its inverse is

$$C_e(t) = h^{-1}(DoH(t); \gamma, C_{e50}, E_0, E_{\max}) = C_{e50}\left(\frac{E_{\max}}{E_0 - DoH(t)} - 1\right)^{-1/\gamma}. \tag{7}$$

Since the parameters are not known with certainty, we will use estimates $\hat{\gamma}$, $\hat{C}_{e50}$, $\hat{E}_0$, $\hat{E}_{\max}$, as explained further in Section 3.2. The blocks $\hat{h}$ and $\hat{h}^{-1}$ in Fig. 1 are thus obtained analogs of (3) and (7). In particular, $\hat{h}^{-1}$ constitutes a linearizing transform, providing a purely measurement-based plasma concentration estimate $\widetilde{C}_e$, used to drive the Kalman filter.

The Kalman filter utilizes the model (2) together with a sequence of sampled input–output data $u, \widetilde{C}_e$ to provide an online estimate $\hat{\boldsymbol{x}}$ of the system state $\boldsymbol{x}$.

Internally, the filter stores its estimate, alongside an error covariance matrix estimate P, which it updates dynamically and uses to compute a gain vector L that is used to drive the estimated state towards the actual one based on model input–output data.

In the following, we present the equations defining the standard Kalman filter. We use $\hat{\boldsymbol{x}}_{k,k-1}$ to denote the estimate of $\boldsymbol{x}_k$, based on data up to and including $k-1$; $\hat{\boldsymbol{x}}_{k,k}$ is the updated estimate incorporating the data sample k. The same double-index notation is used for the covariance estimate P. The update equations for the gain L, covariance P and state estimate $\hat{\boldsymbol{x}}$ are given by

$$L_k = P_{k,k-1}H^\top(HP_{k,k-1}H^\top + R_k)^{-1}, \tag{8a}$$

$$P_{k,k} = (I - L_kH)P_{k,k-1}(I - L_kH)^\top + L_kR_kL_k^\top, \tag{8b}$$

$$\hat{\boldsymbol{x}}_{k,k} = \hat{\boldsymbol{x}}_{k,k-1} + L_k((\widetilde{C}_e)_k - H\hat{\boldsymbol{x}}_{k,k-1}), \tag{8c}$$

$$(\hat{C}_e)_k = H\hat{\boldsymbol{x}}_{k,k}, \tag{8d}$$

while the prediction step is defined by

$$\hat{\boldsymbol{x}}_{k+1,k} = F\hat{\boldsymbol{x}}_{k,k} + Gu_k, \tag{9a}$$

$$P_{k+1,k} = FP_{k,k}F^\top + Q_k, \tag{9b}$$

where F, G, H define the model dynamics according to (4). The measurement equation is given by (8d). The matrices Q and R are the assumed covariances of the additive Gaussian noise, which corrupts the true state $\boldsymbol{x}$ and the output C_e, respectively. Since we only have one measurement signal, R is scalar in our case. Further details, including a derivation of (8) to (9) being optimal in the minimum-variance sense, can be found in [38].

In essence, the Kalman filter combines its prior state estimate with the current measurement to reduce the uncertainty associated with its current state estimate. When the measurement covariance R is large, the Kalman gain is low. Then, the Kalman filter therefore relies more on the model than the measurement for its state estimate update.

The main novelty of our approach is to relate the measurement covariance R to the SQI, to establish a trade-off between measurement and model reliance. We do this by asserting the simple affine relationship

$$R(SQI) = R_{\min} + (R_{\max} - R_{\min})\left(1 - \frac{SQI}{100}\right), \tag{10}$$

where the tuning parameters $R_{\min}$ and $R_{\max}$ define the values of R attained at $SQI = 100$ and $SQI = 0$, respectively. This means that if $SQI = 100$ and the signal quality is perfect, a small value of R, $R_{\min}$, is used. Adversely, if the signal quality is poor with $SQI = 0$, R becomes $R_{\max}$. As the algorithms used to calculate the SQI are proprietary, it is not straightforward to tailor the mapping model from SQI to R. As a first approach, we have opted for a simple linear model to constitute the mapping between SQI and R.

Since our setting lacks process noise as modeled by Kalman covariance Q, we use Q as a constant parameter. For simplicity, we assert a diagonal structure of Q, corresponding to the independent noise added to individual states being mutually independent Gaussians. We therefore consider the four diagonal elements of Q, together with $R_{\min}$ and $R_{\max}$ to be parameters of our filter, where R varies with SQI according to (10).

In our application, we do not have support for the assumption that the process noise is Gaussian. Instead, we consider R and Q as free design parameters of the filter, that are tuned using a population-based approach (that is, using the same values for all the patients) to enable shifting between model and measurement reliance. Therefore, the Kalman filter will not be optimal even though the performance may still be satisfactory. If the noise characteristics at some point will be known to be better described by some other (spectral) noise model, this can be incorporated into the observer design.

The parameters values were optimized offline to minimize the mean square error (MSE) between the simulated patient DoH and the corresponding Kalman filter estimate $\widehat{DoH}$, which is the norm $\mathcal{L}_2$ of $\widehat{DoH} - DoH$. MSE values for each patient were summed, which means that they all contributed equally. The choice of patient population and simulation scenario used in this optimization are those described below in Sections 3.2 and 3.1, respectively. In summary, our design choices are to:

- Optimize $R_{\min}$, $R_{\max}$ and diagonal fixed (time-independent) Q offline to minimize estimation error across a set of simulations (see Section 4);
- Update R online, based on the current SQI, according to (10).

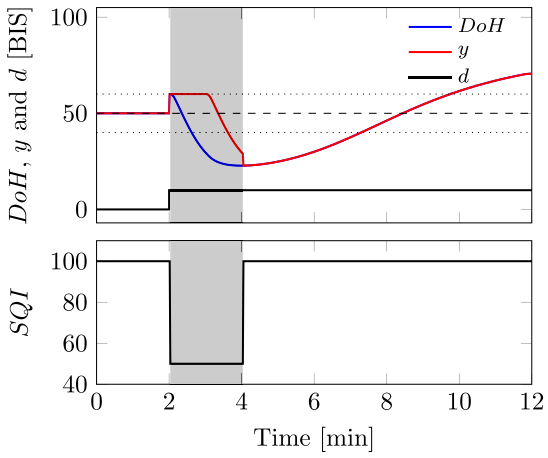

Fig. 2. DoH (top, blue) and monitor output y (top, red). An SQI (bottom, black) drop from 100 to 50 is introduced at $t = 2$ min, and after that, an additive step disturbance $d = 10$ BIS (top, black) occurs. The signal degradation remains during 2 min (shaded area). The associated inference-induced corruption of the monitor output (top, discrepancy between blue and red) is defined in Section 2.3. The dashed black line indicates the DoH reference, and the dotted lines delimit the range between $DoH = 40$ BIS and $DoH = 60$ BIS.

2.3. Monitor

The DoH estimate y, emerging from a clinical monitor, is noisy, even when $SQI = 100$. To reflect this, we use an additive noise model n, as shown in Fig. 1. We will consider both an idealized noise-free case, $n = 0$, and a clinically realistic case, where n is a random cycled noise sequence, recorded by a BIS monitor under stable anesthetic conditions, as explained in [39].

As schematically illustrated in Fig. 1, the (not directly measurable) electro-scalpel inference signal m enters the monitor, where its effect (through an uncharacterized function f) is mapped to SQI. Here, we model this inference with a delay τ that is computed starting from the SQI as

$$\tau = \tau_{\max}\left(1 - \frac{SQI}{100}\right). \tag{11}$$

That is, the inference m affects the SQI and results in the monitor output being delayed from $y(t)$ to $y(t - \tau)$, whenever $SQI < 100$. The delay ranges linearly between $\tau = 0$ s and $\tau = \tau_{\max} = 120$ s, based on SQI. This delay model is consistent with observations of our clinical collaborators and is supported by behavior observed in previous studies, e.g., [24].

In this formulation, the delay of the BIS monitor is not taken into account. We have focused on providing a delay model that describes the degradation of the SQI. Modeling the monitor delay poses a challenge, as the manufacturer has not disclosed the exact response and filtering dynamics of the BIS monitor. Neglecting modeling of the BIS delay has been shown to work in practice, as several clinical studies have been successfully carried out without considering the BIS delay [40,41].

A simulated example of the monitor model is shown in Fig. 2, to illustrate how inference by the electro-scalpel is assumed to affect the monitor and the true DoH, respectively. The blue and red curves in Fig. 2 show the actual DoH, and monitor output y, respectively. The discrepancy is due to the delay model (11) and constitutes the measurement corruption that our soft-sensor approach aims to mitigate the effect. For visual clarity, Fig. 2 shows a scenario with $n = 0$, i.e., in the absence of measurement noise.

2.4. Controller

We use a filtered PID controller [8], which has previously been evaluated in [42]. Its underlying continuous-time transfer function from error e to unsaturated infusion rate $\tilde{u}$ is

$$\frac{\tilde{U}(s)}{E(s)} = K_p\left(1 + \frac{1}{sT_i} + \frac{sT_d}{1 + sT_d/N}\right), \tag{12}$$

with proportional gain $K_p = 0.2$ mg/BIS/s, integral time $T_i = 386$ s, derivative time $T_d = 13.8$ s, and filtering factor $N = 5$. The PID controller values have been obtained by minimizing the integral absolute error (IAE) over a simulation example with additive disturbances, see [42] for details.

The actual infusion rate u is then saturated to within the range 0–1200 $\mathrm{mL\,h^{-1}}$, representative of several clinical infusion pumps. For the concentration of standard propofol solutions of 20 $\mathrm{mg\,mL^{-1}}$, this corresponds to u within the range 0–6.67 $\mathrm{mg\,s^{-1}}$.

3. Comparative simulation study

This section defines the details of our comparative study.

3.1. Surgical scenario

The performance of the proposed control structure was evaluated by repeated simulation of a maintenance phase of fifty minutes of anesthesia. We compare a nominal case, "monitor feedback", with our novel architecture, "soft-sensor feedback". In the monitor feedback case, the soft-sensor block of Fig. 1 was replaced with the moving average filter that was clinically evaluated in connection with the controller of Section 2.4, as described in [43]. This filter averages the eight most recent samples and was used to smooth out the signal.

We study a disturbance scenario to evaluate and compare performance: electro-scalpel activity causes a drop in SQI from 100 to 50, immediately followed by a step disturbance $d = 10$ BIS to reflect a lowered hypnotic depth in the patient resulting from the stimulation. After 2 min, surgical stimulation stops and SQI returns to 100. However, the disturbance $d = 10$ BIS remains, reflecting a lasting nociceptive response. As the actual SQI dynamics are unknown, we have modeled the SQI drop with a double-step since it represents the "worst-case" nature in being abrupt. Moreover, steps are arguably the most common disturbance models considered in the context of closed-loop control systems.

Both the 2 min duration of electro-scalpel stimulation and the associated drop to $SQI = 50$ were derived from data collected during several surgeries. To also investigate the effect of a negative output disturbance step, a second inference episode is initiated with the return from $d = 10$ BIS to $d = 0$ BIS.

The Kalman filter was initialized in the state that corresponds to a DoH of 50 in stationarity, i.e., $x_0 = -F^{-1}Bu_{\mathrm{ref}}$, where u_{ref} is the control signal corresponding to a DoH of 50 in stationarity.

The transients that arise during the initial convergence of the moving average and the Kalman filter, respectively, were truncated from the comparative evaluation. This is realistic, as in clinical use, the filter would typically be activated and allowed to converge before the system is switched from manual to closed-loop drug delivery.

3.2. Patient model population

We have taken both inter- and intra-patient variability into account. This has been achieved by simulating the procedure, detailed in Section 3.1, for 13 distinct individuals with covariates (age, height, weight, sex) and parameter values (E_0, $E_{\max}$, C_{e50}, γ) disclosed in [11], who have already proven to be representative of a broad population. The covariate values were used to obtain a nominal patient model (2) using the Schnider model [29].

For each nominal model, 10 perturbations were obtained by drawing from the associated random effect distributions (5) to reflect model uncertainty caused by variability. Here, it can be noted that different draws were used in the optimization of the Kalman filter, as described in Section 2.2, and the subsequent evaluation simulations.

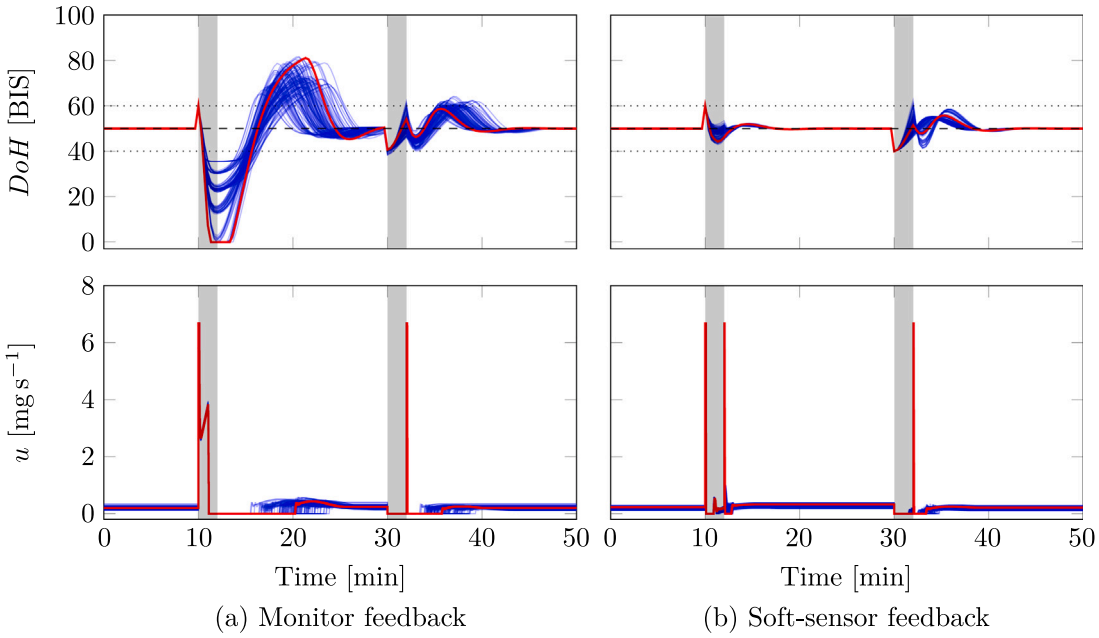

Fig. 3. Blue solid lines represent DoH (upper) and propofol infusion rates (lower) for 10 perturbations of each of 13 nominal patient PKPD model, as explained in Section 3.2. The red solid line represents the mean response obtained for the entire set. According to Section 3.1, a positive step disturbance enters at $t = 10$ min, followed by a negative one at $t = 30$ min. The SQI drops to 50 immediately following each disturbance, before it returns to 100 after 2 min, as indicated by the shaded areas. The dashed black line indicates the DoH reference $r = 50$ BIS, and the dotted lines illustrate the limits of the clinically recommended range between $DoH = 40$ BIS and $DoH = 60$ BIS. Fig. 3(a) corresponds to the nominal case, where feedback is established directly from the monitor measurement; Fig. 3(b) employs feedback from the proposed soft sensor. A representative patient simulation is shown in red for each case.

The Kalman filter incorporates the fixed-effects model only, which introduces a model error between the true patient and the Kalman filter model. The soft-sensor design was also performed without knowledge of E_0, $E_{\max}$, C_{e50}, and γ for each patient in the data set of [11]. Instead, the $\hat{h}^{-1}$ and $\hat{h}$ blocks of the soft sensor (see Fig. 1) were designed on previously published assumed typical values $E_0 = 95.9$ BIS, $E_{\max} = 87.5$ BIS, $C_{e50} = 4.92$ mg L^{-1}, and $\gamma = 2.69$ according to [34].

3.3. Performance evaluation

To evaluate the performance of the proposed control structure, we compared the DoH resulting from a closed loop between the soft-sensor and monitor feedback cases, with and without measurement noise. This comparison was conducted across a population of simulated patients, detailed in Section 3.2.

To evaluate disturbance rejection from the proposed control structure, we used two performance indices, introduced in [44]:

- NADIR: the lowest or highest DoH reached after a positive or negative step disturbance, respectively (indicated by NADIR pos and NADIR neg).
- Time-to-target (TT): the time from step disturbance to first entering the range of 45–55 BIS.

From a clinical point of view, it is interesting to see how well the controller manages to maintain DoH within the 40–60 BIS range, as mentioned, e.g., [45], which was also investigated.

4. Results

Fig. 3 shows DoH resulting from simulating the scenario of Section 3.1 for each of the 130 perturbed patient models according to Section 3.2. The figure corresponds to the noise-free case $n = 0$. Fig. 3(a) shows the results using the conventional monitor feedback approach; Fig. 3(b) shows the results resulting from our novel soft-sensor architecture. The median patient, in terms of DoH reference deviation MSE, is highlighted in red. The Kalman filter parameters used for the simulations in Fig. 3(b) from the optimization described in Section 2.2 are

$$R_{\min} = 5.07 \cdot 10^{-6}, \tag{13a}$$

$$R_{\max} = 0.250, \tag{13b}$$

$$Q = \operatorname{diag}\left(4.79 \cdot 10^{-3}, 0, 1.52 \cdot 10^{-1}, 2.77 \cdot 10^{-4}\right). \tag{13c}$$

Results shown in Fig. 4 are related to simulations performed with the introduction of measurement noise n according to Section 2.3. The Kalman filter parameters, obtained with noise present during the offline optimization phase, were

$$R_{\min} = 0.771, \tag{14a}$$

$$R_{\max} = 1.79, \tag{14b}$$

$$Q = \operatorname{diag}\left(5.79 \cdot 10^{-2}, 1.83 \cdot 10^{-2}, 2.70 \cdot 10^{-2}, 2.12 \cdot 10^{-4}\right). \tag{14c}$$

Fig. 5 shows histograms of the DoH values in Figs. 3 and 4. The percentage of DoH values within the clinically desired 40–60 BIS range in Fig. 5 is 76% for monitor feedback and 100% for soft-sensor feedback without noise. The corresponding values are 71% and 99%, respectively, for the case with noise. Performance measures introduced in Section 3.3 are reported in Table 1.

To evaluate the proposed soft sensor on a wider range of individuals and to show that the tuning of the parameters is effective in general, we study the same simulation scenario as in Fig. 3 over a larger data set of 500 individuals, introduced in [46]. This is shown in Fig. 6.

5. Discussion

We have conducted a comparison between closed-loop DoH control using conventional low-pass filtered monitor output as a feedback signal and a novel soft-sensor architecture that integrates the patient model and the knowledge of signal quality.

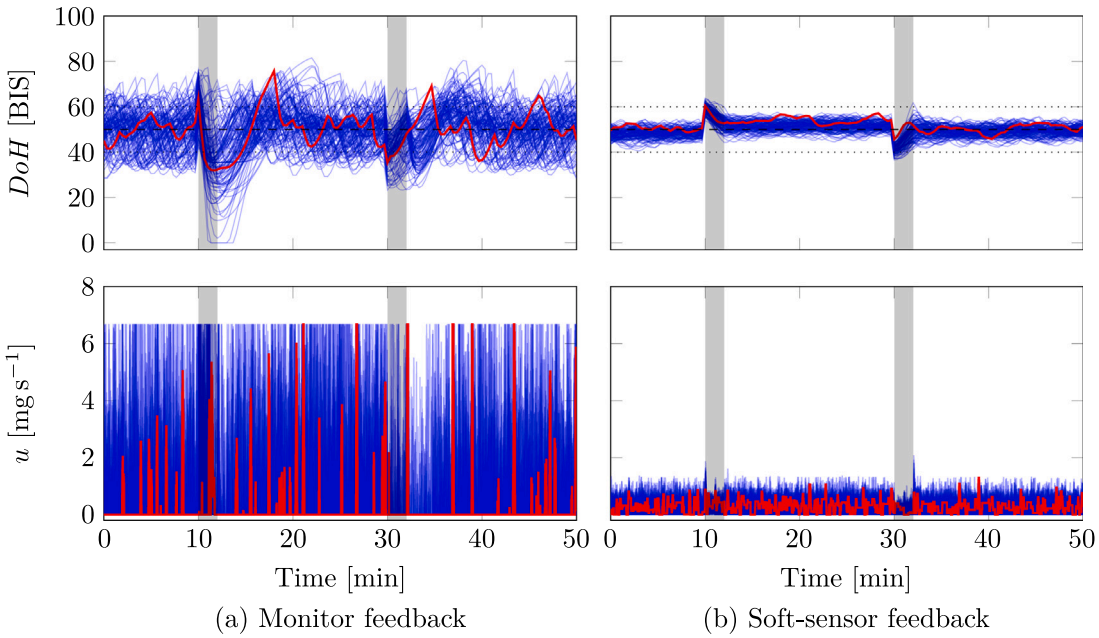

Fig. 4. Simulated *DoH* (upper) and propofol infusion rate (lower) for 130 perturbed patient PKPD models, in the presence of measurement noise. Figure and color content correspond to that of Fig. 3.

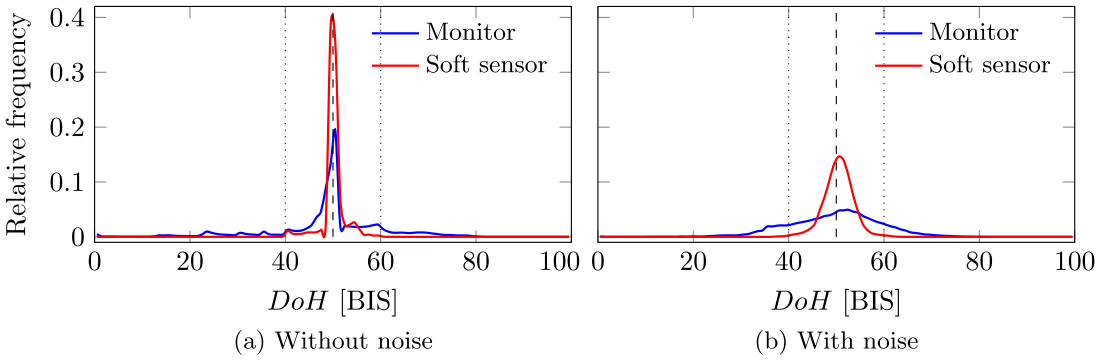

Fig. 5. Distribution of *DoH* values from Figs. 3 to 4, without and with Kalman filter soft sensor in the control loop.

Table 1
Spread of performance measures presented as min–max (median) for the simulations in Figs. 3 to 4.

Feedback	Noise	NADIR pos [BIS]	NADIR neg [BIS]	TT pos [s]	TT neg [s]
Monitor	No	0–35 (23)	57–64 (60)	9–15 (12)	50–106 (65)
Soft sensor	No	43–50 (48)	54–63 (55)	10–21 (14)	49–104 (66)
Monitor	Yes	0–45 (34)	57–81 (65)	0–269 (15)	0–350 (55)
Soft sensor	Yes	44–52 (48)	50–62 (53)	0–264 (70)	0–313 (59)

The performance improvement of our novel architecture over that of the conventional one is perhaps best visualized in the histograms of Fig. 5. They show that the distribution of *DoH* values is more closely centered around the *DoH* maintenance reference $r = 50$ BIS. This is also reflected in the performance indices reported of Table 1. While the difference in time-to-target (TT) between the compared architectures is marginal, the under- and overshoots associated with reaching the target, as well as *DoH* oscillations, differ substantially, as seen in Figs. 3 to 6.

An in-depth effort has been made to ensure realistic simulation circumstances. Instead of assuming perfect model knowledge, which is common in simulation works studying closed-loop control anesthesia, we have adopted a stochastic uncertainty in model parameters, grounded in clinical data [29]. Specifically, we have repeatedly sampled (10 perturbations) from this uncertainty for each of 13 nominal patients defined through population covariate values from a published dataset [11], with the pharmacodynamic parameters of (3). The design of the soft sensor is based solely on assumed knowledge of the nominal model, as described in Section 3.2. Along the same lines, we have used previously published models of surgical disturbance d [21], and measurement noise n [39].

For relating electro-scalpel inference m to SQI, as well as corruption of monitor measurement y, we have formulated our own model (11), as introduced in Section 2.3. This has been done based on communication with our senior anesthesiologist collaborator, who has observed a delay in monitoring reporting following such inference. We believe that the fidelity of this simple model could be improved upon. However, its sole purpose in the current context is to provide a substantial corruption of the monitor output y, which is reflected in SQI. The fact that the inference signal m in our simple model is directly mapped to $SQI =$

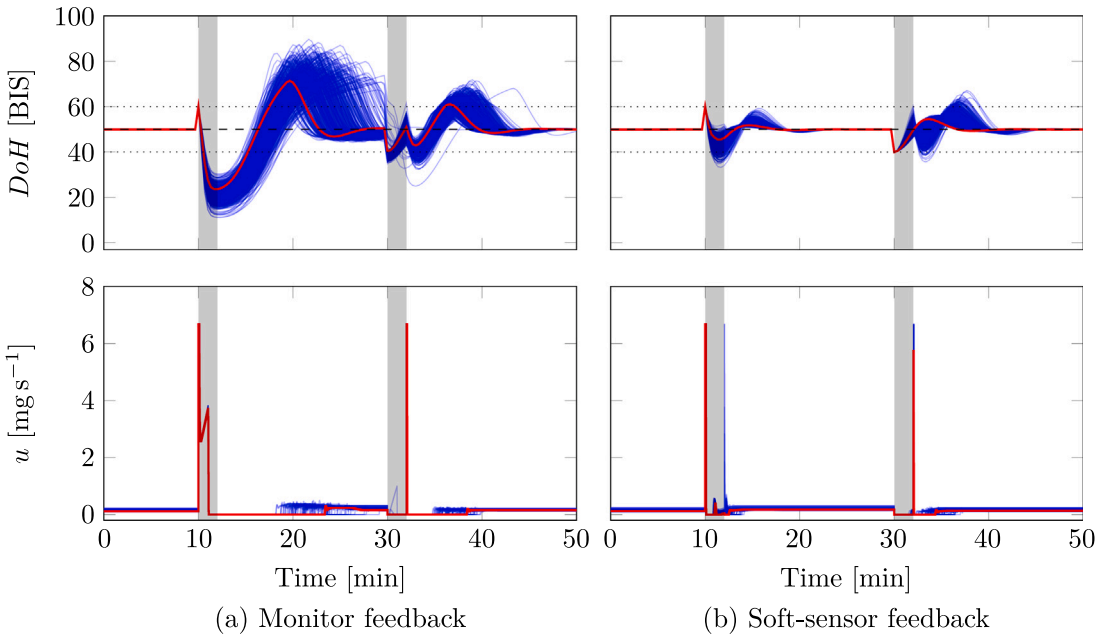

Fig. 6. Simulated DoH (upper) and propofol infusion rate (lower) for 500 patient PKPD models to evaluate how the soft sensor handles inter-patient variability on a larger data set from [46]. Figure and color content correspond to that of Fig. 3.

m is just a matter of convenience for notation. Neither this nor the knowledge about how SQI therefore relates to the delay τ through (11) has been exploited in the soft-sensor design. Instead, the soft sensor assumes only that the measurement uncertainty — in terms of variance R of an additive Gaussian measurement noise — is an affine function of SQI, according to (10), mapping the 100–0 SQI range to an R_{min}–R_{max} range. Thus, the soft sensor is agnostic of the monitor dynamics mapping inference m to corruption on y, which is later reported by the SQI. Although the monitor dynamics are not taken into account in the proposed architecture, the performance is satisfactory. Doing so would be unrealistic, even if the performance could be slightly improved.

Another implication is that our methodology can be expected to work satisfactorily not only with the BIS monitor but also other clinical monitors, such as the WAV_{CNS} [47] or CONOX [48], that output both a DoH estimate y and associated SQI.

On a similar note, our Kalman filter assumes signal corruption by Gaussian noise added to the signal $\widetilde{C}_e$ in Fig. 1. At least for the noise contribution of n to this signal, a more accurate model could be incorporated. Also, here, satisfactory performance in the absence of such a model is positive, since it demonstrates that a low-fidelity noise model is sufficient for our architecture to outperform the nominal one with simple monitor feedback. While more advanced sensor fusion methods like the extended or unscented Kalman filters could be considered in scenarios where the model is not linear like in (1), the simple linear Kalman filter already provides significant performance improvements. Its simplicity and interpretability make it an attractive choice for real-world implementation unless there is a strong motivation for more complex alternatives.

Some of the residual error arising from model mismatch is accounted for by the process noise model Q. Like with R, the underlying assumed noise structure does not match exactly that of the considered system. However, optimizing R and (an assumed diagonal) Q according to Section 2.2 yields satisfactory performance. To implement this soft-sensor in practice, R_{min}, R_{max} and Q would be optimized offline, with R then adjusted online based on (10).

6. Conclusions

A realistic closed-loop controlled anesthesia scenario is considered, in which model uncertainties and external disturbances are present. In this setting, our comparative simulation study clearly illustrates robust performance benefits from merging a model-based and data-driven approach through a Kalman filter soft sensor. In particular, it enables online balance between model and measurement reliance, based on an estimation of measurement quality.

Based on the results presented, we are confident to take the next steps toward the clinical evaluation of the proposed soft-sensor architecture within an existing clinical closed-loop anesthesia research platform, which to date has seen extensive clinical use [43,49].

CRediT authorship contribution statement

Ylva Wahlquist: Writing – review & editing, Writing – original draft, Visualization, Software, Methodology. **Nicola Paolino:** Writing – review & editing, Writing – original draft, Software, Methodology, Conceptualization. **Michele Schiavo:** Writing – review & editing, Validation, Methodology, Conceptualization. **Antonio Visioli:** Writing – review & editing, Validation, Supervision, Conceptualization. **Kristian Soltesz:** Writing – review & editing, Validation, Supervision, Conceptualization.

Declaration of competing interest

The authors declare that they have no known competing financial interests or personal relationships that could have appeared to influence the work reported in this paper.

Acknowledgments

The authors would like to acknowledge Massimiliano Paltenghi with the Department of Anesthesiology, Critical Care and Emergency, Spedali Civili di Brescia, Brescia, Italy for sharing his clinical expertise on the relationship between electric inference and monitor dynamics.

Wahlquist and Soltesz are members of the ELLIIT Strategic Research Area at Lund University. This work was partially supported by the European Union NextGeneration EU (Piano Nazionale di Ripresa e Resilienza (PNRR) - Missione 4 componente 2, investimento 3.3 - Decreto del Ministero dell'Università e della Ricerca n.352 del 09/04/2022). Paolino has been partially funded by CSMT Innovative Contamination Hub.

Data availability

No data was used for the research described in the article.

References

[1] M.R. Blayney, Procedural sedation for adult patients: an overview, Continuing Educ. Anaesth. Crit. Care Pain 12 (4) (2012) 176–180, http://dx.doi.org/10.1093/bjaceaccp/mks016.

[2] A.R. Absalom, J.I.B. Glen, G.J.C. Zwart, T.W. Schnider, M.M.R.F. Struys, Target-controlled infusion: a mature technology, Anesth. Analg. 122 (1) (2016) 70–78, http://dx.doi.org/10.1213/ANE.0000000000001009.

[3] I.J. Rampil, A primer for EEG signal processing in anesthesia, Anesthesiology 89 (1998) 980–1002, http://dx.doi.org/10.1097/00000542-199810000-00023.

[4] J. Vuyk, M. Mertens, Bispectral index scale (BIS) monitoring and intravenous anaesthesia, Adv. Model. Clin. Appl. Intraven. Anaesth. (2003) 95–104, http://dx.doi.org/10.1007/978-1-4419-9192-8_9.

[5] M. Ghita, M. Neckebroek, C. Muresan, D. Copot, Closed-loop control of anesthesia: survey on actual trends, challenges and perspectives, IEEE Access 8 (2020) 206264–206279, http://dx.doi.org/10.1109/ACCESS.2020.3037725.

[6] M. Hosseinzadeh, K. van Heusden, M. Yousefi, G.A. Dumont, E. Garone, Safety enforcement in closed-loop anesthesia. A comparison study, Control Eng. Pract. 105 (2020) 104653, http://dx.doi.org/10.1016/j.conengprac.2020.104653.

[7] J. Agarwal, G.D. Puri, P.J. Mathew, Comparison of closed loop vs. manual administration of propofol using the bispectral index in cardiac surgery, Acta Anaesthesiol. Scand. 53 (3) (2009) 390–397, http://dx.doi.org/10.1111/j.1399-6576.2008.01884.x.

[8] A. Visioli, Practical PID Control, Springer Science & Business Media, ISBN: 978-1-84628-585-1, 2006.

[9] G.A. Dumont, A. Martinez, J.M. Ansermino, Robust control of depth of anesthesia, Internat. J. Adapt. Control Signal Process. 23 (5) (2009) 435–454, http://dx.doi.org/10.1002/acs.1087.

[10] J.M. Gonzalez-Cava, F. Bagge Carlson, O. Troeng, A. Cervin, K. van Heusden, G.A. Dumont, K. Soltesz, Robust PID control of propofol anaesthesia: uncertainty limits performance, not PID structure, Comput. Methods Programs Biomed. 198 (2021) 105783, http://dx.doi.org/10.1016/j.cmpb.2020.105783.

[11] F. Padula, C. Ionescu, N. Latronico, M. Paltenghi, A. Visioli, G. Vivacqua, Optimized PID control of depth of hypnosis in anesthesia, Comput. Methods Programs Biomed. 144 (2017) 21–35, http://dx.doi.org/10.1016/j.cmpb.2017.03.013.

[12] G.D. Puri, B. Kumar, J. Aveek, Closed-loop anaesthesia delievery system (CLADS) using bispectral index; a performance assessment study, Anaesth Intensive Care. 35 (2007) 357–362, http://dx.doi.org/10.1177/0310057X0703500306.

[13] K. Soltesz, J. Hahn, T. Hägglund, G.A. Dumont, J.M. Ansermino, Individualized closed-loop control of propofol anesthesia: a preliminary study, Biomed. Signal Process. Control 8 (6) (2013) 500–508, http://dx.doi.org/10.1016/j.bspc.2013.04.005.

[14] L. Merigo, M. Beschi, F. Padula, N. Latronico, M. Paltenghi, A. Visioli, Event-based control of depth of hypnosis in anesthesia, Comput. Methods Programs Biomed. 147 (2017) 63–83, http://dx.doi.org/10.1016/j.cmpb.2017.06.007.

[15] L. Merigo, F. Padula, N. Latronico, M. Paltenghi, A. Visioli, Event-based control tuning of propofol and remifentanil coadministration for general anaesthesia, IET Control Theory Appl. 14 (19) (2020) 2995–3008, http://dx.doi.org/10.1049/iet-cta.2019.1067.

[16] A. Pawlowski, M. Schiavo, N. Latronico, M. Paltenghi, A. Visioli, Linear MPC for anesthesia process with external predictor, Comput. Chem. Eng. 161 (2022) 107747, http://dx.doi.org/10.1016/j.compchemeng.2022.107747.

[17] D. Copot, C. Muresan, R. De Keyser, C. Ionescu, Patient specific model based induction of hypnosis using fractional order control, IFAC-PapersOnLine 50 (1) (2017) 15097–15102, http://dx.doi.org/10.1016/j.ifacol.2017.08.2238.

[18] N. Paolino, M. Schiavo, N. Latronico, F. Padula, M. Paltenghi, A. Visioli, On the use of FOPID controllers for maintenance phase of general anesthesia, Appl. Sci. 13 (2023) 7381, http://dx.doi.org/10.3390/app13137381.

[19] J.A. Mendez, A. Marrero, J.A. Reboso, A. Leon, Adaptive fuzzy predictive controller for anesthesia delivery, Control Eng. Pract. 46 (2016) 1–9, http://dx.doi.org/10.1016/j.conengprac.2015.09.009.

[20] J.A. Mendez, A. Leon, A. Marrero, J.M. Gonzalez-Cava, J.A. Reboso, J.I. Estevez, J.F. Gomez-Gonzalez, Improving the anesthetic process by a fuzzy rule based medical decision system, Artif. Intell. Med. 84 (2018) 159–170, http://dx.doi.org/10.1016/j.artmed.2017.12.005.

[21] K. Soltesz, K. van Heusden, G. Dumont, Models for control of intravenous anesthesia, Automated Drug Delivery in Anesthesia, Elsevier, Amsterdam, Netherlands, ISBN: 9780128159750, 2019, pp. 119–156, http://dx.doi.org/10.1016/B978-0-12-815975-0.00010-2,

[22] BIS™ complete monitoring system, Medtronic, Minneapolis, Minnesota, U.S, 2013, URL https://asiapac.medtronic.com/content/dam/covidien/library/global/multi/product/brain-monitoring/BISCompleteMonitor_OperatorsManual_Multi_10103075A00.pdf.

[23] A. Dahaba, Different conditions that could result in the bispectral index indicating an incorrect hypnotic state, Anesth. Analg. 101 (3) (2005) 765–773, http://dx.doi.org/10.1213/01.ane.0000167269.62966.af.

[24] M. Chan, S.S. Ho, T. Gin, Performance of the bispectral index during electrocautery, J. Neurosurg. Anesthesiol. 24 (1) (2012) 9–13, http://dx.doi.org/10.1097/ANA.0b013e31823058bf.

[25] E. Gjika, M. Pekker, A. Shashurin, M. Shneider, T. Zhuang, J. Canady, M. Keidar, The cutting mechanism of the electrosurgical scalpel, J. Phys. D: Appl. Phys. 50 (2) (2016) 025401, http://dx.doi.org/10.1088/1361-6463/50/2/025401.

[26] V. Oikonomou, A. Tzallas, S. Konitsiotis, D. Tsalikakis, D. Fotiadis, The use of Kalman filter in biomedical signal processing, in: Kalman Filter Recent Advances and Applications, IntechOpen, 2009, http://dx.doi.org/10.5772/6805.

[27] B.J.E. Misgeld, M. Luken, R. Riener, S. Leonhardt, Observer-based human knee stiffness estimation, IEEE Trans. Biomed. Eng. 64 (5) (2017) 1033–1044, http://dx.doi.org/10.1109/TBME.2016.2587841.

[28] B. Aubouin-Pairault, M. Fiacchini, T. Dang, Comparison of multiple Kalman filter and moving horizon estimator for the anesthesia process, J. Process Control 136 (2024) 103179, http://dx.doi.org/10.1016/j.jprocont.2024.103179.

[29] T.W. Schnider, C.F. Minto, P.L. Gambus, C. Andresen, D. Goodale, S. Shafer, E.J. Youngs, The influence of method of administration and covariates on the pharmacokinetics of propofol in adult volunteers, Anesthesiology 88 (5) (1998) 1170–1182, http://dx.doi.org/10.1097/00000542-199805000-00006.

[30] K.J. Åström, R.M. Murray, Feedback systems: An introduction for scientists and engineers, Princeton University Press, Princeton, NJ, ISBN: 978-0-691-13576-2, 2008.

[31] M.M.R.F. Struys, T. De Smet, B. Depoorter, L.F.M. Versichelen, E.P. Mortier, F.J.E. Dumortier, S.L. Shafer, G. Rolly, Comparison of plasma compartment versus two methods for effect compartment–controlled target-controlled infusion for propofol, Anesthesiology 92 (2) (2000) 339, http://dx.doi.org/10.1097/00000542-200002000-00021.

[32] S. Goutelle, M. Maurin, F. Rougier, X. Barbaut, L. Bourguignon, M. Ducher, P. Maire, The Hill equation: A review of its capabilities in pharmacological modelling, Fundam. Clin. Pharmacol. 22 (6) (2008) 633–648, http://dx.doi.org/10.1111/j.1472-8206.2008.00633.x.

[33] K.J. Åström, B. Wittenmark, Computer Controlled Systems: Theory and Design, third ed., Dover Publications, Mineola, NY, ISBN: 978-0-486-48613-0, 2011.

[34] A. Vanluchene, H. Vereecke, O. Thas, E. Mortier, S. Shafer, M. Struys, Spectral entropy as an electroencephalographic measure of anesthetic drug effect: A comparison with Bispectral Index and processed midlatency auditory evoked response, Anesthesiology 101 (2004) 34–42, http://dx.doi.org/10.1097/00000542-200407000-00008.

[35] J.A. Canchola, S. Tang, P. Hemyari, E. Paxinos, E. Marins, Correct use of percent coefficient of variation (%CV) formula for log-transformed data, MOJ Proteomics Bioinform. Volume 6 (Issue 4) (2017) http://dx.doi.org/10.15406/mojpb.2017.06.00200.

[36] U. Melia, E. Gabarron, M. Agusti, N. Souto, P. Pineda, J. Fontanet, M. Vallverdu, E.W. Jensen, P. Gambus, Comparison of the qCON and qNOX indices for the assessment of unconsciousness level and noxious stimulation response during surgery, J. Clin. Monit. Comput. 31 (2017) 1273–1281, http://dx.doi.org/10.1007/s10877-016-9948-z.

[37] G. Welch, G. Bishop, An Introduction to the Kalman Filter, Tech. Rep., University of North Carolina, 1995, http://dx.doi.org/10.5555/897831.

[38] A. Becker, Kalman Filter: From the Ground Up, First edition, ISBN: 978-965-598-439-2, 2023.

[39] A. Pawlowski, M. Schiavo, N. Latronico, M. Paltenghi, A. Visioli, MPC for propofol anesthesia: the noise issue, in: 2022 IEEE Conference on Control Technology and Applications, CCTA, 2022, pp. 1087–1092, http://dx.doi.org/10.1109/CCTA49430.2022.9966102.

[40] N. Liu, T. Chazot, A. Genty, A. Landais, A. Restoux, K. McGee, P. Laloe, B. Trillat, L. Barvais, M. Fischler, Titration of propofol for anesthetic induction and maintenance guided by the bispectral index: Closed-loop versus manual control: A prospective, randomized, multicenter study, Anesthesiology 104 (4) (2006) 686–695, http://dx.doi.org/10.1097/00000542-200604000-00012.

[41] M.M.R.F. Struys, T. De Smet, L.F.M. Versichelen, S. Van de Velde, R. Van den Broecke, E.P. Mortier, Comparison of closed-loop controlled administration of propofol using bispectral index as the controlled variable versus standard practice controlled administration, Anesthesiology 95 (1) (2001) 6–17, http://dx.doi.org/10.1097/00000542-200107000-00007.

[42] M. Schiavo, F. Padula, N. Latronico, M. Paltenghi, A. Visioli, Individualized PID tuning for maintenance of general anesthesia with propofol, IFAC-PapersOnLine 54 (3) (2021) 679–684, http://dx.doi.org/10.1016/j.ifacol.2021.08.320.

[43] M. Schiavo, F. Padula, N. Latronico, L. Merigo, M. Paltenghi, A. Visioli, Performance evaluation of an optimized PID controller for propofol and remifentanil coadministration in general anesthesia, IFAC J. Syst. Control 15 (2021) 100121, http://dx.doi.org/10.1016/j.ifacsc.2020.100121.

[44] C.M. Ionescu, R. De Keyser, B.C. Torrico, T. De Smet, M. Struys, J.E. Normey-Rico, Robust predictive control strategy applied for propofol dosing using BIS as a controlled variable during anesthesia, IEEE Trans. Biomed. Eng. 55 (9) (2008) 2161–2170, http://dx.doi.org/10.1109/TBME.2008.923142.

[45] K. Soltész, On Automation in Anesthesia (Ph.D. thesis), Lund University, Lund, Sweden, ISBN: 978-91-7473-484-3, 2013.

[46] M. Schiavo, L. Consolini, M. Laurini, N. Latronico, M. Paltenghi, A. Visioli, Optimized feedforward control of propofol for induction of hypnosis in general anesthesia, Biomed. Signal Process. Control 66 (2021) 102476, http://dx.doi.org/10.1016/j.bspc.2021.102476.

[47] J.O. Hahn, G.A. Dumont, J.M. Ansermino, Robust closed-loop control of hypnosis with propofol using WAV_{CNS} index as the controlled variable, Biomed. Signal Process. Control 7 (5) (2012) 517–524, http://dx.doi.org/10.1016/j.bspc.2011.09.001.

[48] E.W. Jensen, J.F. Valencia, A. Lopez, T. Anglada, M. Agusti, Y. Ramos, R. Serra, M. Jospin, P. Pineda, P. Gambus, Monitoring hypnotic effect and nociception with two EEG-derived indices, qCON and qNOX, during general anaesthesia, Acta Anaesthesiol. Scand. 58 (8) (2014) 933–941, http://dx.doi.org/10.1111/aas.12359.

[49] M. Schiavo, F. Padula, N. Latronico, M. Paltenghi, A. Visioli, A modified PID-based control scheme for depth-of-hypnosis control: Design and experimental results, Comput. Methods Programs Biomed. 219 (2022) 106763, http://dx.doi.org/10.1016/j.cmpb.2022.106763.